Small angle x-ray scattering to investigate the specific surface of hydrated alginate microbeads

F. Ghernaouti, Aurélie Perrin, J. Causse, Fabrice Chandre, D. Cornu, J. Cambedouzou

Small angle x-ray scattering to investigate the specific surface of hydrated alginate microbeads

F. Ghernaouti[1,#], A. Perrin[2,#], J. Causse[3], F. Chandre[2], D. Cornu[1] and J. Cambedouzou[1,*]

[1] IEM, Univ Montpellier, CNRS, ENSCM, Montpellier, France.
[2] MIVEGEC, Univ Montpellier, CNRS, IRD, Montpellier, France
[3] ICSM, Univ Montpellier, CEA, CNRS, ENSCM, Marcoule, France

[#] Equally contributed to this work
[*] Corresponding author; email: julien.cambedouzou@enscm.fr

Abstract

Encapsulation of active substances in biopolymer beads becomes a widely developed approach to gain efficiency for many applications. However, the characterization of such aqueous materials in their early stage of production is very delicate regarding their textural properties. The classical tools such as gas adsorption and Hg porosimetry can hardly provide relevant information since they require the removal of water, which is yet a fundamental part of the sample that drives its structure. In this article, we used small angle x-ray scattering (SAXS) as a tool in order to determine the specific surface area (SSA) of alginate microbeads in solution. This has been made possible by a careful procedure of SAXS measurements, involving calibration samples, allowing writing intensities in absolute units. Therefore, the Porod limit theory was used to calculate the SSA from the scattering length contrast and the measured absolute intensity. In addition, we compared the SSA of microbeads obtained from pure water and from a widely used cell culture medium, and we followed the textural evolution of a water alginate sample during the first step of a gentle drying process. Our results show that SAXS should be considered as a valuable tool for physico-chemists and food formulators in order to extract in situ dimensional and textural information of hydrogels during the formulation. It enables them to figure out the real surface available for the sorption of additive or active molecules in the formulation of biopolymers such as alginates, empowering them to better control encapsulation processes.

Keywords: alginate beads, texture analysis, small angle scattering, specific surface area

1. Introduction

Encapsulation makes it possible to protect an active substance from the environment by trapping inside a material for a tunable duration, and to keep this substance until it is released at a given time and/or at a given location. The number of active substances and of protective encapsulating materials is huge. Among the examples highlighting the importance of such an approach in healthcare applications, one can cite e.g. protection of RNA molecules inside lipid bilayer nanoparticles used in CoViD-19 vaccines (Ickenstein & Garidel, 2019), subcutaneous implants for delayed delivery of drugs

in the organism (Roberge et al., 2020), or storage of drugs in alginate beads (Uyen, Hamid, Tram, & Ahmad, 2020). The latter example in itself refers to tens of different molecules with various indications, loaded in alginate compounds that represent a material for encapsulation with wide potential of uses. In particular, the food industry introduced alginates as textural agents for their thickening and antioxidants properties. Under the form of microbeads, they can be used as encapsulating agents for flavors [Bouwmeesters & De Roos, 2005]. Studying the textural properties of these beads is of prime importance in order to better control the release of these agents.

When trying to determine the structural properties of alginate beads, some features involving the size and concentration of the beads, the chemical composition, and their surface functions are easily determined using characterization techniques such as optical microscopy, dynamic light scattering and optical spectroscopy. However, when it is about other features such as textural characteristics (pore size, porosity, specific surface area), the determination becomes much more complicated because commonly used characterization techniques (electron microscopy, gas sorption experiments, Hg porosimetry) become inappropriate. They indeed require a vacuum step that leads to evacuation of water or solvent from the structure of these gels, which necessarily modifies the microstructure of the sample. Many ways of removing the solvent have been considered, involving oven drying, cryo-lyophylisation and CO_2 supercritical drying, but they all result, albeit in different proportions, to a modification of the sample microstructure (Rodríguez-Dorado et al., 2019; Veronovski, Tkalec, Knez, & Novak, 2014). Consequently, these techniques cannot give a relevant information about the texture of the hydrated material, whose actual structure seems out of reach. Fortunately, other characterization techniques based on completely different physical phenomena can provide valuable information in this situation.

When applied to complex soft materials as alginates beads in solution, beam/matter interaction theory provides a formalism that not only allows a quantitative determination of structural features such as the size and shape of nano-objects and their typical distance, but also provides access to textural information. Among these are the relative volume of the aqueous phase with respect to that of the alginate phase, and the specific surface area (here defined as the quantity of interface normalized to the volume of sample probed). These determinations are based on the use of the so-called invariant theorem and the Porod's limit theorem, respectively. Their use is conditioned by a very careful treatment of the experimental data derived from small angle x-ray scattering (SAXS) experiments, allowing the experimenters to write the intensity in absolute units, and the determination of the scattering length of each phase constituting the medium. Such an approach has been used for aerogels (Bugnone, Ronchetti, Manna, & Banchero, 2018; Dieudonné, Delord, & Phalippou, 1998) and mesoporous silica (Cambedouzou & Diat, 2012), but was never described in detail for fully hydrated alginate microbeads.

In this article, we provide a detailed analysis of two samples of alginate microbeads obtained by electrospraying two separate solutions of sodium alginate of the same batch, but involving only water in one case and a more complex aqueous solution used as a cell culture medium in the other case. The latter choice was motivated by the growing interest in encapsulating biomolecules of pharmaceutical interest produced by mammalian or insect cells in alginate beads. In a rationalized production set-up, it can be envisioned to i) remove cells from the cell culture medium after bioproduction, ii) add alginate salt in the cell culture solution containing biomolecules, and iii) fabricate the beads encapsulating biomolecules. Therefore, the study of alginate beads synthesized from such a complex solution makes sense. Both solutions were electrosprayed in a bath of $CaCl_2$ solution. Our analyze based on SAXS/Wide Angle X-ray Scattering (WAXS) experiments shows that a specific surface area can be derived in both cases, highlighting a similar bulk texture for the two samples despite different morphologies revealed by surface analyzes. In addition, the measurements carried out on a similar sample after a drying step under mild conditions shows an increased specific surface area and the emergence of micropores.

2. Materials and Methods

The alginate microbeads in water were obtained by electrospraying a solution of 1.3 wt. % sodium alginate (CAS 9005-38-3) purchased from Sigma Aldrich in MilliQ water at a constant speed of 2.1 $mL \cdot s^{-1}$. The alginate beads were reticulated in a 0.2M solution of $CaCl_2$. The solution of alginate microbeads in water is further denoted AW.

The second sample, called AC, was obtained from a complex solution of sodium alginate and Roswell Park Memorial Institute (RPMI 1640) based cell culture medium. RPMI medium is used as culture medium for a wide diversity of mammalian or insect cells. The complex solution considered here has been used in order to grow insect cells that were further eliminated by successive clarification and ultracentrifugation steps. The electrospraying protocol was identical to the one used for the AW sample.

Optical microscopy measurements were carried out on a Keyence VHX-7000 microscope. Scanning electron microscopy was performed on a Zeiss EVO HD15.

SAXS/WAXS experiments were carried out in the transmission geometry of a laboratory set-up available at the Institut de Chimie Séparative de Marcoule, France, involving a XENOCS molybdenum anode and a Fox-3D monochromator delivering a 17.4 keV monochromatic beam of dimension 800x800 μm^2 after collimation by two sets of antiscattering slits. The detection is made by a MAR345 imaging plate detector. In this set-up, the scattering vectors available range from 0.2 to 30 nm^{-1}. The corresponding d values in the real space are smaller than 30 nm, which is enough to study the structure of nanopores and mesopores in the samples. However, information at a larger scale that could be derived from lower q-range, *e.g.* slopes related to the fractal structure of larger objects such as in

Tomchuk et al. 2020 for example, is not reachable with this set-up. Samples were measured in glass capillaries of diameter 2mm (Hilgenberg, glass no. 14). These capillaries remain at ambient pressure and temperature, i.e. no vacuum fluctuation could perturb the samples during the experiment. Each acquisition duration is 30 min, and was repeated 5 times in order to gain signal to noise ratio. The total duration of each acquisition is therefore 2.5h on each sample. All diagrams were plotted separately before compilation (data addition for the same collection angle finally denoted $I_{S+EC}^{exp}(q)$) in order to check the reproducibility and rule out ageing effects such as sedimentation. Standard calibration was made involving a silver behenate sample to determine accurately the detector center and the sample to detector distance. SAXS intensity calibration was made by measuring a Goodfellow® polyethylene sample of width 2.36 mm, for which the absolute intensity is known (4.9 cm^{-1} at scattering vector q = 0.37 nm^{-1}), giving access to an experimental factor E_f involving the x-ray flux, the detector efficiency and the solid angle of detection (Schaffer & Hendricks, 1974). The raw SAXS profile of this calibration sample is shown as supplementary information in Figure SI1. In order to perform the cleanest sample correction as possible, we measured separately empty glass capillaries for the same duration than the samples (5 times 30 minutes). The experimental intensity of these glass capillaries is denoted $I_{EC}^{exp}(q)$. The transmission *T* of all samples and empty capillary was calculated by dividing the photon count on a photodiode through the object in the beam by the photon count in the absence of the object. All SAXS intensities were converted in absolute units ($I_S^{abs}(q)$) normalized to the width *w* of the sample holder according to equation (1):

$$I_S^{abs}(q) = \frac{1}{E_f \cdot w}\left(\frac{I_{S+EC}^{exp}(q) - n \cdot 8}{T_{S+EC} \cdot t_{S+EC}} - \frac{I_{EC}^{exp}(q) - n \cdot 8}{T_{EC} \cdot t_{EC}}\right) \qquad (1)$$

where n represents the number of added acquisitions for each sample (n.8 being the total number of counts due to the reading procedure of the imaging plate), the *S* index stands for sample and the *EC* index stands for the Empty Capillary. Finally, *t* is the total duration of the acquisition. An example of such data treatment is exemplified for pure water as supplementary information, in Figure SI2.

3. Results and Discussion

Two different samples of electrosprayed alginates beads were synthesized. The first one, called AW, results from a solution of sodium alginate in water. It is expected to contain only crosslinked calcium alginate and water. The second one, called AC, was obtained from a solution of sodium alginate in a common cell culture medium representative of the experimental conditions used to culture mammalian and insect cells (Moore & Woods, 1976). This solution was taken from an actual insect cell culture medium after purification. As a result, it might contain a variety of macromolecules in addition to water and reticulated calcium alginate.

Figure 1 shows the morphology of sample AW and AC as imaged by optical microscopy, in their liquid synthesis medium and after partial drying; the latter will be further referred to as AWD. A higher magnification is given by the scanning electron microscopy (SEM) images, but the material endured a severe degassing before observation, leading to a drastic drying of any adsorbed water molecule.

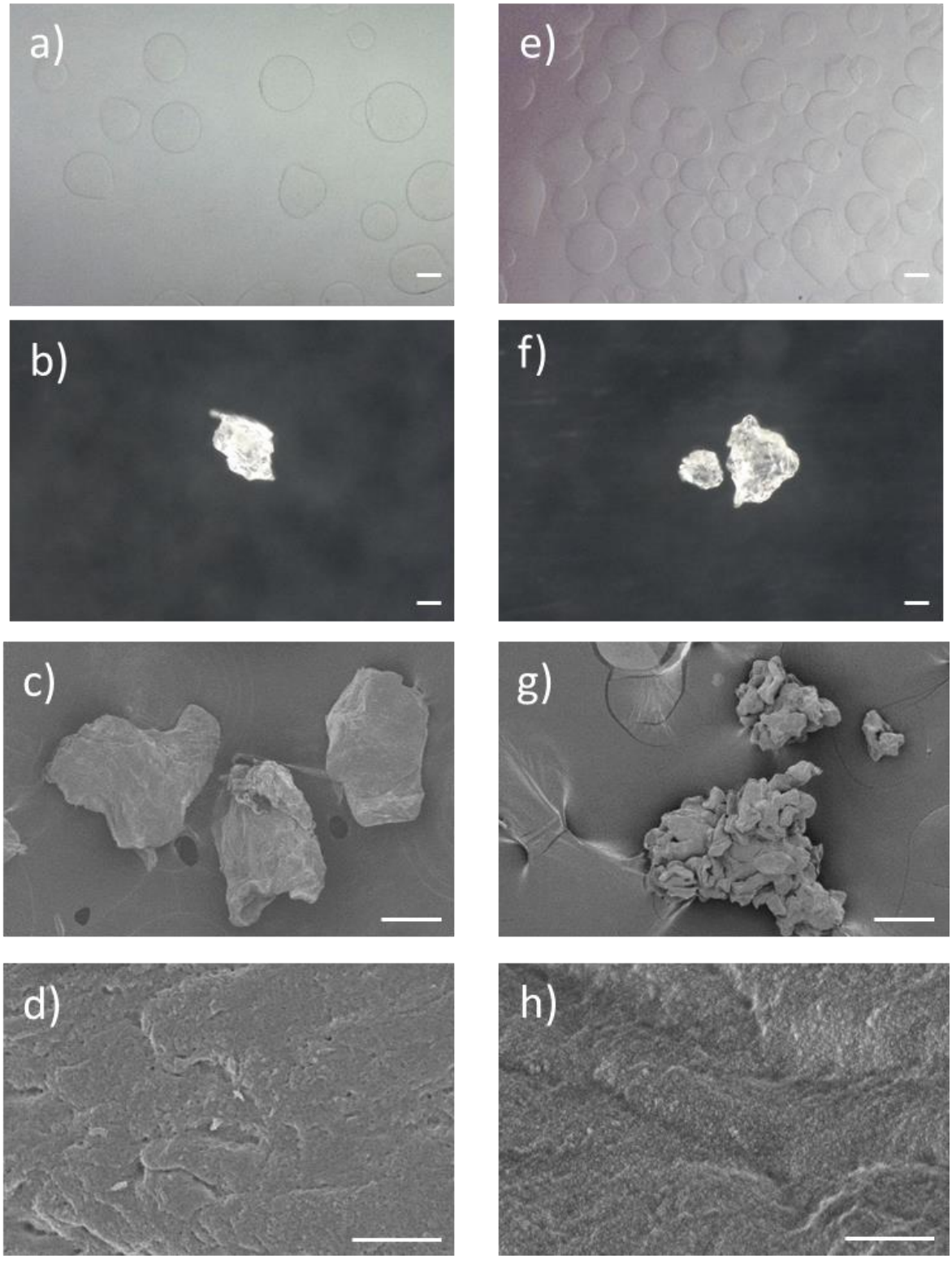

Figure 1. Microscopy images of AW (a-d) and AC (e-h). Optical microscopy in solution (a,e), after ambient temperature drying overnight (b,f). SEM images at dried beads at low magnification (c,g) and of their surface at high magnification (d,h). Scale bar is 100 µm in (a,b,e,f), and 1 µm in (d,h).

Optical microscopy images of the microbeads obtained from the two different solutions show samples of similar spherical shape and size, with diameter ranging from 100 to 400 micrometers, with a mean value of 250 µm ± 50 µm for AW and 200 µm ± 50 µm for AC. When observed after one night of drying under ambient pressure and controlled temperature (25°C ± 1°C), optical microscopy images clearly reveal an expected loss of the spherical shape upon drying, suggesting major structural and textural changes inside the samples. However, a remaining quantity of water inside the pores of both samples prevented us from measuring their textural properties by gas adsorption experiments nor Hg porosimetry. Finally, SEM images confirm the amorphization of the shape of the microbeads upon further degassing. The observation of the SEM images of the highest magnification reveals a rough surface morphology, which seems more pronounced in the AC sample. The characteristic size of the roughness is difficult to measure precisely, but it can be estimated between 100 and 300 nm. This morphology could be associated to the pore connection with the surface, but this has to be confirmed by textural measurements.

In order to overcome this limitation in the measurement of the texture of the humid samples, we took advantage of the possibilities offered by SAXS in the structural analyzes of such samples. Figure 2a shows the SAXS profiles of the AW and AC samples, in absolute units after proper correction of the sample holder signal versus scattering vector q, as described in the previous section. The profiles of pure water and of the RPMI-based medium are added. Concerning the water SAXS profile, we can notice that the intensity when q tends to 0 is of about $1.6.10^{-2}$ cm^{-1}, in good agreement with the theoretical value calculated using the isothermal compressibility of water, i.e. $1.65.10^{-2}$ cm^{-1} (Orthaber, Bergmann, & Glatter, 2000). The RPMI solution displays density inhomogeneity at the scale of more than 30 nm, as revealed by the intensity increase at small angles, probably due to the presence of small impurities (cell fragments...) that were not removed by the purification step before collecting the solution.

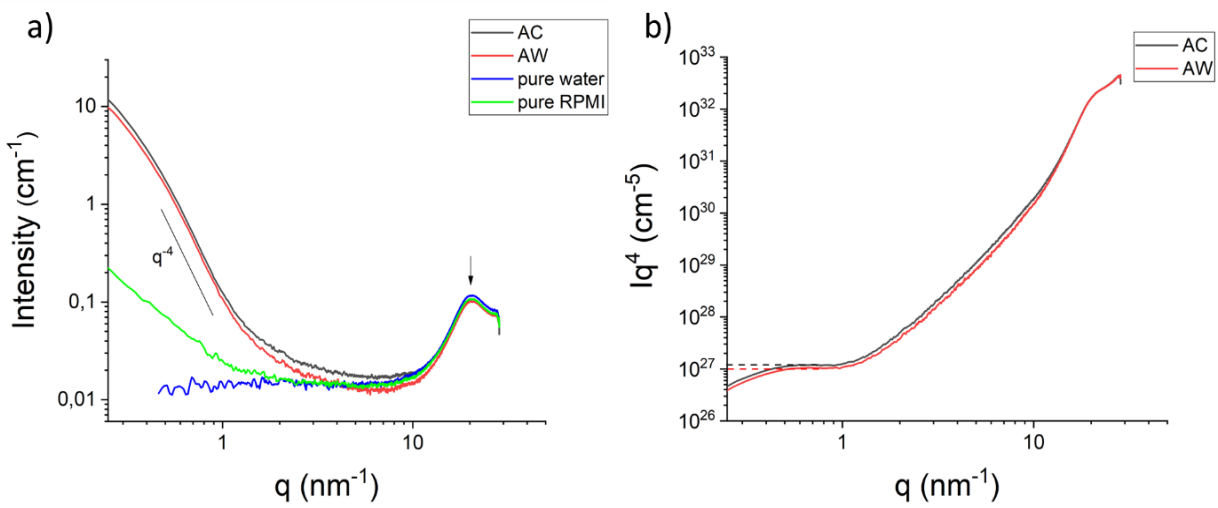

Figure 2. a) SAXS profiles of samples AC, AW, pure water and pure RPMI-based medium. The arrow points toward the feature characteristic of intermolecular distance of water, and the black line follows a q^{-4} law. b) Porod plots of samples AC and AW. The dashed lines materialize the value of Iq^4 when q tends to 0 for AC (black) and AW (red).

The AC and AW samples show a similar profile over the whole probed q-range, testifying to a very similar structure. In particular, the feature at 20 nm^{-1} (rather belonging to the wide angle x-ray scattering or "diffraction" range), which corresponds to the mean distance between oxygen atoms in liquid water and can therefore be considered as characteristic of the intermolecular distance in liquid water (Hura et al., 2003; Yahya et al., 2020), presents a perfect intensity match in both samples. This indicates that the proportion of water is roughly identical in both samples. Concerning the lower q-range, both samples show a strong signal at low angles, likely attributable to pores larger than 30 nm, the latter value being the higher limit of the object size accessible with our set-up. Note that the AC signal is not strongly impacted by the diffusion from the objects contained in the RPMI solution, as the amplitude of their scattering is between one and two order of magnitude smaller from the AC signal. Moreover, the intensity decreases in both samples according to a q^{-4} power law, characteristic of a so-called Porod regime, i.e. the pore interface between the water or RPMI medium and the alginate matrix is sharp [Porod 1]. In these samples roughly constituted by two phases (aqueous phase and reticulated alginate) presenting a contrast of electron density, and a sharp interface between them, it is possible to apply the so-called theorem of the Porod limit (Porod, 1951 ; Porod, 1982), writing as :

$$(Iq^4) = 2\pi(\Delta\rho)^2\Sigma \qquad (2)$$

where Δρ represents the contrast of scattering length density between the two phases, and Σ represents the volume quantity of interface, corresponding to the specific surface area expressed in surface/volume units, typically $cm^2 \cdot cm^{-3}$.

Transforming the experimental data into the Porod representation (Figure 2b) leads the Porod regimes to appear as horizontal lines in the plot. Such horizontal domains are observed in both curves in Fig. 2b, and a projection on the vertical axis was made along the dashed lines in Fig. 2b. The $(Iq^4)_{q\to 0}$ values for AW and AC are respectively of $1.06 \pm 0.05 \cdot 10^{27}$ cm^{-5} and $1.19 \pm 0.05 \cdot 10^{27}$ cm^{-5}. The estimation of the uncertainties is based on the cumulated errors arising from the fluctuation of the x-ray source and the noise level on the Porod plot. The conversion of these values into a specific surface area requires a reliable estimate of the local density of the alginate walls. Such a determination is rather difficult to achieve, so we propose here a theoretical determination, in which we start from the volume mass of dry calcium alginate ($2.1\ g \cdot cm^{-3}$)(Chemical Book, 2021), and from its molecular formula, i.e. $C_{18}H_{24}CaO_{19}$ (National Center for Biotechnology Information, 2021). Note that this extreme hypothesis, in which no water intercalates in the bulk structure of calcium alginate, will result in a minimum value for the specific surface area of the material. Taking into account the atomic masses and the Avogadro number, it is possible to calculate a tentative electron density equal to 0.51 electron per cubed Angstrom. This number, once multiplied by the classical electron radius ($2.82 \cdot 10^{-13}$ cm), gives the scattering length density of alginate equal to $1.85 \cdot 10^{11}$ cm^{-2}.

In order to define error bars within the same hypothesis, we could alternatively consider that the molecular formula of sodium alginate is $C_{12}H_{14}CaO_{12}$ (Food Chemical Codex, 2004) and determine, following the same path than above, that the scattering length density of calcium alginate equals to $1.81 \cdot 10^{11}$ cm^{-2}. Therefore, a value of $1.83 \pm 0.02 \cdot 10^{11}$ cm^{-2} could be considered here.

Considering the scattering length density of water equal to $9.38 \cdot 10^{10}$ cm^{-2} (Henke, Gullikson, & Davis, 1993), the contrast of scattering length density between water and calcium alginate is $\Delta\rho = 8.9 \pm 0.2 \cdot 10^{10}$ cm^{-2}. It is then straightforward to derive the specific surface area in AW and AC from equation (2), i.e. $2.1 \pm 0.2 \cdot 10^4$ $cm^2 \cdot cm^{-3}$ and $2.4 \pm 0.2 \cdot 10^4$ $cm^2 \cdot cm^{-3}$, respectively. It is therefore possible to extrapolate a value in m^2 per gram in order to compare qualitatively this result with those obtained by gas adsorption measurements, keeping in mind that this comparison is artificial since our materials in the present state cannot be studied with the latter technique. Considering the volume mass of dry calcium alginate given above, and that beads occupy 74% of the volume (hypothesis of a compact packing of spheres) one finds specific surface areas of 1.3 ± 0.1 and 1.5 ± 0.2 $m^2 \cdot g^{-1}$ for the AW and AC sample, respectively.

These values of specific surface areas are in line with values expected for a macroporous material, which could also be exemplified as spheres of radius 1.3-1.5 µm of calcium alginate of bulk density 2.1. These specific surface area values are two order of magnitude away those reported in textural studies

based on gas adsorption analyzes achieved on dried alginate powders (Rodríguez-Dorado et al., 2019). For example, Rodriguez et al reported typical specific surface areas in alginate aerogels and xerogels ranging from 100 to 500 $m^2 \cdot g^{-1}$, with typical pore diameters in the 10 to 30 nm range.

While very different, these results obtained in the present study are not incompatible with results from the literature, because they do not concern materials taken in the same state. As explained above, gas adsorption measurements require dried sample, in which water was eliminated. Researchers have tried many ways of withdrawing water in order not to destroy the morphology of the hydrated compound. However, in highly hydrophilic samples as polysaccharides, the elimination of water is necessarily driving structural reorganization that change the textural properties of the material. In particular, the high surface area measured by gas adsorption technique on freeze dried samples testifies to the presence of micropores connected with the exterior of alginate beads, that we did not detect by SAXS in the liquid phase and that could have been created during the water vapor escape from the inner part of the beads.

In order to go further with the drying process of alginate beads and the corresponding structural changes, we performed another measurement on a sample of alginate beads dried for 24h at ambient temperature. This dried alginate sample (denoted as AWD) is under the form of a humid white powder. An optical microscopy image of the AWD sample is shown in Fig. 1b. It is obvious that alginate beads have lost their spherical morphology, suggesting important textural transformations. We therefore performed a SAXS experiment on this sample, and we compared its SAXS profile with that of the fully hydrated AW sample in Figure 3a.

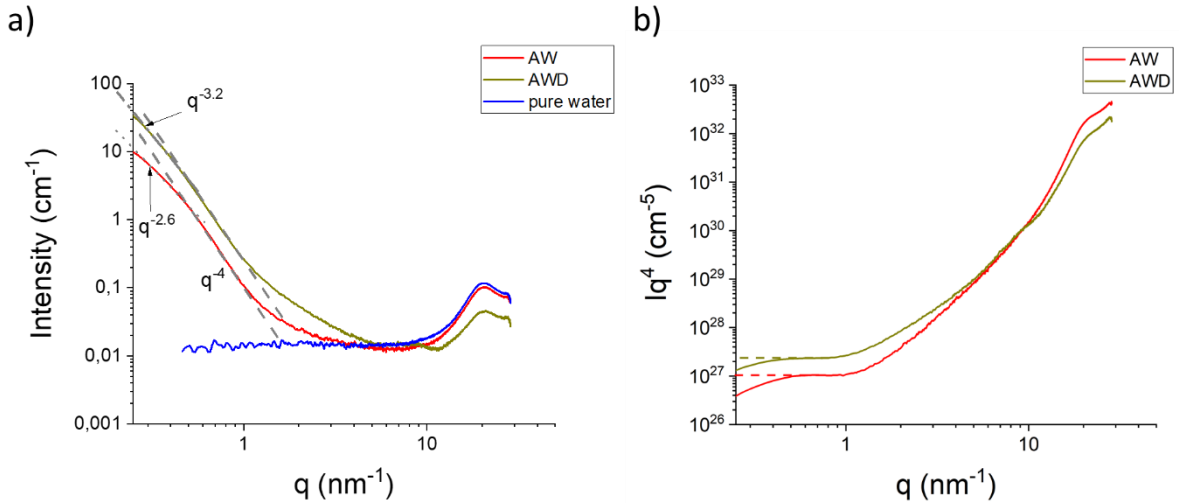

Figure 3. a) SAXS profiles of samples AW, AWD, and pure water. Dashed and dotted lines highlight power laws measured in the low scattering vectors region. b) Porod plots of samples AW and AWD. The dashed lines materialize the value of Iq^4 when q tends to 0 for AW (red) and AW (dark yellow).

The intensity profile of the AWD sample shows marked differences with that of AW. In the higher q range, the feature at 20 nm^{-1} characteristic of intermolecular distances in water has sensibly decreased, in good agreement with the loss of a part of water due to the drying process. It is reasonable to think that the inter-bead water was removed during the drying process, but that there is still water in the porous structure of alginate grains. We measured the transmission of the AWD sample (T_{AWD}=0.85), and compared it to that of the AW sample (T_{AW} = 0.75). The transmission of the AW sample may be expressed as follows:

$$T_{AW} = e^{-\mu_{water} \cdot x_{wag} - \mu_{water} \cdot x_{wip} - \mu_{alg} x_{alg}} = e^{-\mu_{water} \cdot x_{wag}} \cdot T_{AWD} \qquad (3)$$

where μ_{water} and μ_{alg} are respectively the lineic mass absorption coefficient of water and alginate, and x_{wag}, x_{wip} and x_{alg} are respectively the width of the layer of water around grains, water in pores and alginate. Considering the lineic mass absorption of water at 17.5 keV of 1.08 cm^{-1} (National Institute of Standards and Technology, 2021), we can extrapolate a x_{wag} of 0.12 cm, and finally an inter-grain volume fraction of 62% considering the width of the sample holder (1.95mm). This is more than twice (2.3) larger than the 26% we considered in the ideal case of a compact packing of spheres, however it remains an overestimated value since additional water could be present in the new porous structure of beads that have endured structural transformation upon drying. In the following, we will keep the hypothesis of compact packing of spheres in order to compare with the results obtained on the AW sample.

In the SAXS profile of AWD sample, the loss of intensity in higher q range due to the elimination of a part of the water in the sample is associated to an increase of the overall intensity in the low q-range. The intensity increase is the largest for q values around 1 to 3 nm^{-1}, corresponding to typical distances of 2 to 3 nm, which could correspond to newly created micropores. At the lowest scattering vectors accessible, i.e. between 0.25 and 0.5 nm^{-1}, an increase of the slope from $q^{-2.6}$ to $q^{-3.3}$ can be measured. Although a fine understanding of the pore morphology is out of reach here, this increase of the power law describing the intensity decrease in the low scattering vectors range might be attributed to an evolution of the mean shape of the pores for typical lengths of 15 - 25 nm from a planar character to a more spherical character. This could refer to an increase in the curvature of the pores. Skipping to Porod representation, it can be seen that a Porod regime still exists in the AWD sample, and the intensity of the plateau domain is slighly higher than for the AW sample ($2.51 \pm 0.05 \cdot 10^{27}$ cm^{-5} versus $1.06 \pm 0.05 \cdot 10^{27}$ cm^{-5}). Considering that all the pores that can be probed in this SAXS experiment remain filled with water, we can use the same value than for the AW sample for the scattering length density contrast in order to estimate the specific surface area using Equation 2. It comes that the specific surface area in AWD is $4.8 \pm 0.2 \cdot 10^4$ $cm^2 \cdot cm^{-3}$, corresponding to 2.3 ± 0.2 $m^2 \cdot g^{-1}$ and to a picture of non-porous alginate spheres of radius 630 ± 30 nm. These values are estimated for an ideal packing density of spheres, which is probably overestimated, making the estimation of the specific surface area

a lower limit. In a rough first approximation, taking into account a not compact packing and a volume fraction of water equal to 0.62 instead of 0.26, as described above for the AWD sample, the specific surface area would reach 5.3 $m^2.g^{-1}$. Overall, these results show that the drying of the alginate beads, monitored by the decrease of the signal characteristic of bulk water, is accompanied by an increase of the specific surface area and the emergence of new nanometric typical distances that are in line with the appearance of micropores. The methodology described in this article could then be adapted in order to follow the structure evolution of beads during an *in situ* experiment of sample progressive drying. Finally, the use of this methodology allows knowing the quantity of interface by volume unit in the liquid phase, i.e. directly during the elaboration of calcium alginate beads. It will enable researchers to have a better idea of the real surface available for the sorption of additive or active molecules in the formulation of alginates, and thus will help them improving their process.

4. Conclusion

Small Angle X-ray Scattering (SAXS) was used in order to reveal structural and textural information on hydrated alginate microbeads that are out of reach for classical gas adsorption methods, requiring a preliminary water drying of the sample that consequently transform the structure of these highly hydrophilic samples. Comparing the structure of two samples in gel phase made from two distinct water solutions (pure water and a cell culture medium), and applying the formalism of the Porod limit theorem, we showed that the specific surface area of both samples did not significantly change depending on the water phase. A specific surface area of about 1.3 ± 0.1 $m^2.g^{-1}$ was found, in line with a macroporous structure, and far below the values given by gas adsorption of samples after freeze-drying or other preparation techniques. The same measurements were carried out on a sample partially dried under ambient conditions for 24 hours, and it was found that the specific surface area increased by a twofold factor. Moreover, the SAXS profile of the latter sample shows a signal that could be attributed to the emergence of a microporosity. These results demonstrate the benefit of SAXS techniques in order to access the actual texture of samples that can hardly be studied by gas adsorption or electron microscopy without pre-treatments drastically modifying their structure. Besides, it is important to take into account that the change in the porous structure of the beads due to drying might influence the release of the active principles introduced in the beads during the formulation. Finally, this methodology will allows researchers to quantify the interface per volume unit during the formulation step of calcium alginate beads, and therefore represents a valuable tool to understand the loading of additives that could be inserted in alginate beads directly during their synthesis.

Acknowledgements

The authors acknowledge Université de Montpellier through the "KIM RIVE" project for financial support. The authors thank D. Cot and B. Rebiere for their help on microscopy techniques.

References

Bouwmeesters, J.F., & De Roos, K.B. (2005). Process for preparing beads as food additive and product thereof, US Patent N°USOO692.9814B2.

Bugnone, C.A., Ronchetti, S., Manna, L., & Banchero, M. (2018). An emulsification/internal setting technique for the preparation of coatedand uncoated hybrid silica/alginate aerogel beads for controlled drug delivery. *Journal of Supercritical Fluids, 142*, 1-9. https://doi.org/10.1016/j.supflu.2018.07.007.

Cambedouzou, J., & Diat O. (2012). Quantitative small-angle scattering on mesoporous silica powders: from morphological features to specific surface estimation, *Journal of Applied Crystallography, 45*, 662-673. https://doi.org/10.1107/S0021889812020298.

Chemical Book. (2021). Database for CAS 9005-35-0 compound: Calcium alginate. Retrieved July 7, 2021 from https://www.chemicalbook.com/ChemicalProductProperty_EN_cb1438558.htm

Dieudonné, P., Delord, P., & Phalippou, J. (1998). Small angle X-ray scattering of aerogel densification, *Journal of Non-Crystalline Solids, 225*, 220–225. https://doi.org/10.1016/S0022-3093(98)00120-3.

Food Chemical Codex. (2004). *Calcium alginate*. p. 11. Institute of Medicine: National Academies Press. 5th Edition.

Henke, B.L., Gullikson, E.M., & Davis, J.C. (1993). X-ray interactions: photoabsorption, scattering, transmission, and reflection at E=50-30000 eV, Z=1-92, *Atomic Data and Nuclear Data Tables, 54(2)*, 181-342.

Hura, G., Russo, D., Glaeser, R.M., Head-Gordon, T., Krack, M., & Parrinello, M. (2003). Water structure as a function of temperature from X-ray scattering experiments and ab initio molecular dynamics, *Phys. Chem. Chem. Phys.*, *5*, 1981–1991. https://doi.org/10.1039/B301481A.

Ickenstein, L.M., & Garidel, P. (2019). Lipid-based nanoparticle formulations for small molecules and RNA drugs. *Expert Opinion on Drug Delivery, 16(11)*, 1205-1226. https://doi.org/10.1080/17425247.2019.1669558.

Moore, G.E., & Woods, L.K. (1976). Culture Media for Human Cells- RPMI 1603, RPMI 1634, RPMI 1640 and GEM 1717. *Tissue Culture Association Manual, 3*, 503-508. https://doi.org/10.1007/BF00918753.

National Center for Biotechnology Information. (2021). PubChem Compound Summary for CID 44630049, Calcium alginate. Retrieved July 7, 2021 from https://pubchem.ncbi.nlm.nih.gov/compound/Calcium-alginate

National Institute of Standards and Technology. (2021). Retrieved July 7, 2021 from https://physics.nist.gov/PhysRefData/FFast/html/form.html

Orthaber, D., Bergmann, A. & Glatter, O. (2000). SAXS experiments on absolute scale with Kratky systems using water as a secondary standard. *Journal of Applied Crystallography, 33*, 218–225. https://doi.org/10.1107/S0021889899015216.

Porod, G. (1951). Die Röntgenkleinwinkelstreuung von dichtgepackten kolloiden Systemen. *Kolloid-Zeitschrift, 124*, 83–114. https://doi.org/10.1007/BF01512792.

Porod, G. (1982). In *Small Angle X-ray Scattering*, edited by O. Glatter & O. Kratky, pp. 17-51. New York: Academic Press.

Roberge, C., Cros, J.M., Serindoux, J., Cagnon, M.E., Samuel, R., Vrlinic, T., Berto, P., Rech, A., Richard, J., & Lopez-Noriega, A. (2020). BEPO (R): Bioresorbable diblock mPEG-PDLLA and triblock PDLLA-PEG-PDLLA based in situ forming depots with flexible drug delivery kinetics modulation. *Journal of Controlled Release, 319*, 416-427. https://doi.org/10.1016/j.jconrel.2020.01.022.

Rodríguez-Dorado, R., López-Iglesias, C., García-González, C.A., Auriemma, G., Aquino, R.P., & Del Gaudio, P. (2019). Design of Aerogels, Cryogels and Xerogels of Alginate: Effect of Molecular Weight, Gelation Conditions and Drying Method on Particles' Micromeritics. *Molecules, 24*, Article 1049. https://doi.org/10.3390/molecules24061049.

Schaffer, L.B., & Hendricks, R.W. (1974). Calibration of Polyethylene (Lupolen) as a Wavelength-Independent Absolute Intensity Standard. *J. Appl. Cryst., 7*, 159-163. https://doi.org/10.1107/S0021889874009009.

Tomchuk, O.V., Avdeev, M.V., Aksenov, V.L., Shulenina, A.V., Ivankov, O.I., Ryukhtin, V., Vékás, L., & Bulavin, L.A. (2021). Temperature-dependent fractal structure of particle clusters in aqueous ferrofluids by small-angle scattering. *Colloids and Surfaces A: Physicochemical and Engineering Aspects*, *613*, Article 126090. https://doi.org/10.1016/j.colsurfa.2020.126090.

Uyen, N.T.T., Hamid, Z.A.A., Tram, N.X.T., & Ahmad. (2019) N. Fabrication of alginate microspheres for drug delivery: A review. *International Journal of Biological Macromolecules, 153*, 1035-1046. https://doi.org/10.1016/j.ijbiomac.2019.10.233.

Veronovski, A., Tkalec, G., Knez, Z., & Novak Z. (2014). Characterisation of biodegradable pectin aerogels and their potential use as drug carriers. *Carbohydrate Polymers, 113*, 272-278. https://doi.org/10.1016/j.carbpol.2014.06.054.

Yahya, A., Tan, L., Perticaroli, S., Mamontov, E., Pajerowski, D., Neuefeind, J., Ehlers, G., & Nickels, J.D. (2020). Molecular origins of bulk viscosity in liquid water. *Phys. Chem. Chem. Phys., 22*, 9494. https://doi.org/10.1039/D0CP01560A.